TO: **Texas Hazardous Waste Research Center)**

FROM: **Dr. Danny Reible**
University of Texas (now Texas Tech University)
danny.reible@ttu.edu/806-834-8050

SUBJECT: **Final Project Report**

PROJECT NUMBER:

PROJECT TITLE: Coupling of Produced Water Treatment and Flare Recovery in Unconventional Oil and Gas Production

PROJECT PERIOD: 9/1/13-8/31/14

DATE: **9/16/14**

A Preliminary Simulation of Membrane Distillation for Treatment of Hydraulic Fracturing Produced Waters

by

Lily Xu

B.S., Massachusetts Institute of Technology (2012)

Submitted to the Department of Environmental and Water Resources Engineering in fulfillment of the requirements for the degree of

Master of Science in Environmental and Water Resources Engineering

at the

UNIVERSITY OF TEXAS AT AUSTIN

under the guidance of Dr. Danny Reible and Dr. Helen Lou

December 13, 2013

Acknowledgements

I wish to express my sincere gratitude to Dr. Danny Reible of the University of Texas at Austin and to Dr. Helen Lou of Lamar University for their invaluable guidance and support. This project would not have been possible without them. A special thanks goes to Dr. Chauchyun Chen of Texas Tech University, whose direction was instrumental in the formulation of this work. I would also like to express gratitude to Joseph Chen for his patience and motivation; Xiaolong Shen for his enthusiasm in problem-solving and generosity in sharing it; Jennifer Wang for her cheerleading; Roxana Darvari for her support and Persian food; and Cyrus Vafadari for his love of heat exchangers.

Abstract

Hydraulic fracturing, the process most responsible for the boom in the shale gas industry, generates an enormous amount of water. These waste waters are the largest volumetric byproduct streams associated with the fracturing process. Only a fraction of these waters are treated and reused, while a great deal is disposed in injection wells or as surface discharge. Another environmental complexity associated with hydraulic fracturing involves the flaring of gas, an embodiment of increased carbon dioxide emissions and wasted energy. This project aims to investigate the water-energy nexus and to develop a strategy that can address both the water management and reduction of flared gas issue using an optimal design of a produced water treatment system. This particular study will use membrane distillation, an emerging desalination technology that can utilize low-grade heat sources like flared gas to drive mass transport, for the conceptual process design. A preliminary MATLAB simulation of membrane distillation suggests that the module is most effective when operating at the highest allowable feed inlet temperature. A preliminary flowsheet of a multistage operation was also constructed in Aspen Plus. This simulation is characterized by 10 stages and composed of a series of feed flash-evaporation and absorption blocks. The recovery ratio, a system performance indicator, was found to be 4.1%, indicating a high rate of conversion from feed to permeate waters. Future avenues for exploration in these preliminary simulations are a must and will include investigations into energy efficiency and water production costs associated with different operating variables.

Contents

List of Figures

1 Introduction

This project aims to investigate the water-energy nexus in waste water management and to develop strategies that can collectively address the water management issue and reduce the amount of wasted flared gas in natural gas extraction. Hydraulic fracturing is a process used in the extraction of shale gas that generates an enormous amount of water. Once an injection cycle has been completed, the hydraulic pressure is reduced, and a cocktail of fluids are returned to the surface. These fluids include not only the extracted gas but also waste waters, which are by far the largest volumes of byproduct streams associated with natural gas exploration. Fakhru'l-Razi et al. estimates that global produced water generation is around 250 million barrels per day [1]. On a global scale, only a fraction of this produced water is treated and reused in the hydraulic fracturing process. Instead, must of the water is disposed by surface discharge or injection into underground disposal wells, although these proportions are dependent on geology and geography [2]. Thus, the economic productivity of shale gas reservoirs depends heavily on the success of its management and development of cost-effective water treatment technologies for these waters.

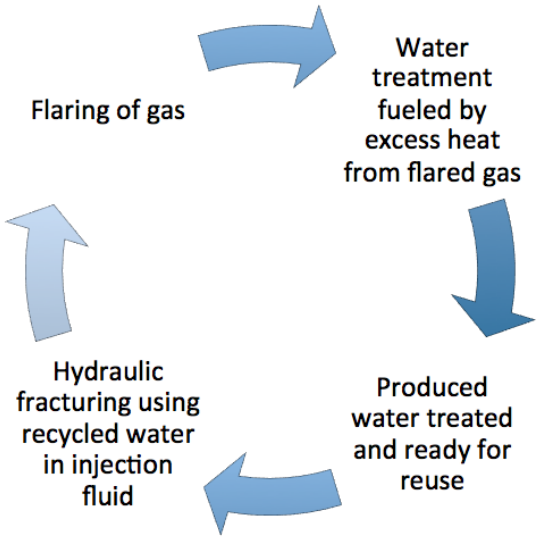

Figure 1: A synergetic strategy.

Gas flaring is another harmful byproduct associated with hydraulic fracturing. These flares were originally designed as precautionary measures for over-pressurized equipment [3]; however, a great deal of the gas flaring observed today has little to do with emergency prevention but rather with shale production economics, especially at a well site's initiation. Gas flaring is extremely common in areas lacking proper gas processing plant capacity and gasline infrastructure [4]. Additionally, the low value of gas as compared to oil minimizes the in-

centive to truck the gas using more valuable oil. Naturally, there is a growing commercial interest in recovering and utilizing the heat energy lost during gas flaring.

As shown in Fig. 1., the intended strategy proposes a water management scheme that couples the treatment of produced waters while also harnessing the flared gas energy. In this synergetic system, the flaring of gas, which would otherwise function as excess wasted heat, would provide the energy to propel the water treatment process. The resulting treated water can then be recycled as injection fluid for the next hydraulic fracturing cycle.

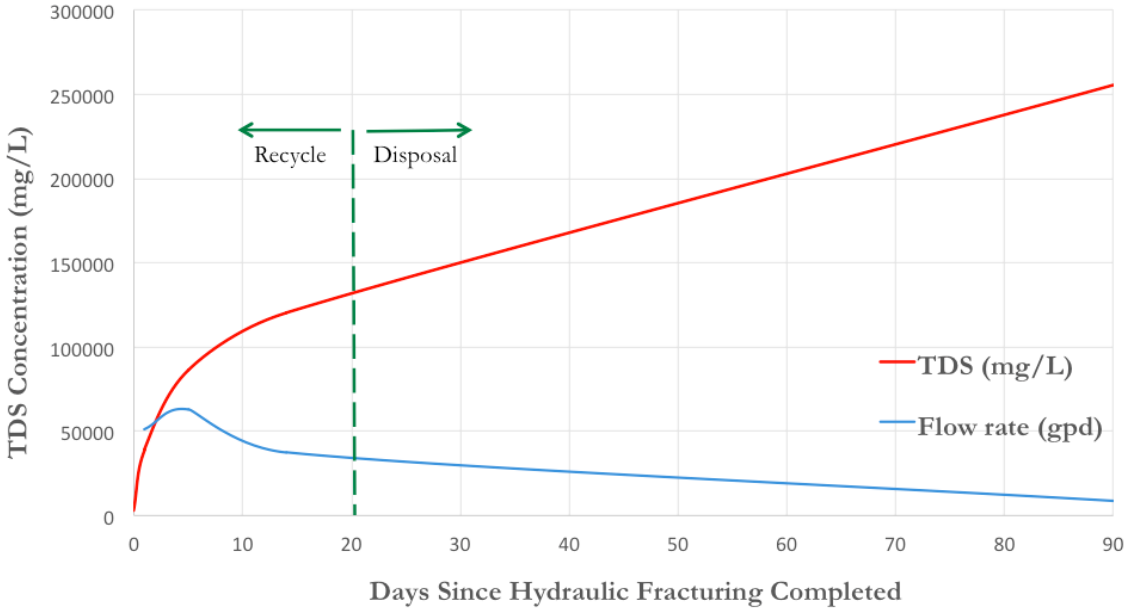

Figure 2: Average flowback TDS concentration and discharge rate [5].

Produced waters, or waters that previously existed in formation, can be marked by exceptionally high concentrations of total dissolved solids (TDS), especially after an injection cycle has been completed for some period of time. Fig. 2. illustrates how the average TDS concentration and discharge rate of produced and flowback waters change over time since hydraulic fracturing has been completed [5]. The flowback water, composed mostly of injection fluids, returns to the surface during the initial 10 days and has a pretty low TDS concentration. The discharge rate is strongest during the early period since reduction of fracturing injection pressure has just occurred. The TDS concentration gradually increases over time as more of the produced water begins to emerge from the well, reaching up to 200,000 mg/L depending on geology [10]. The saline produced waters can be very difficult to manage, treat, could potentially create significant environment damange if mismanaged.

Shale gas operators must make an important water management decision based on the economics of desalination and choose when to recycle by treating and reusing and when to dispose. The illustrated green recycle-disposal line in Fig. 2. serves only as a guideline and shifts depending on geology and geography of shale play. For example, this line will shift to the right for the Marcellus Shale Formation since its geology is not suitable for injection wells and its formation waters are prone to concentrations of TDS up to 190,000 mg/L [2]. Conversely, for the Barnett Shale, disposal by injection is a cost effective disposal method as there are over 12,000 Class II injection wells in Texas [6]. A map illustrating the locations of active shale plays in the U.S. and their respective TDS concentrations are shown in Fig. 3.

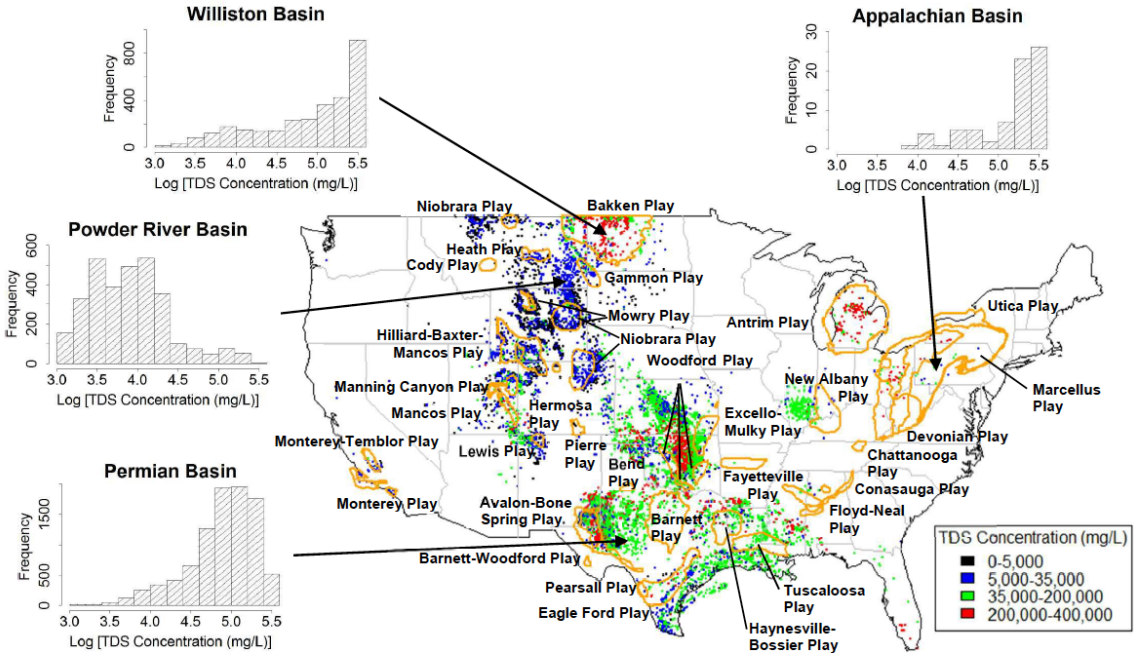

Figure 3: Map of active U.S. shale plays in the U.S. and respective TDS concentrations [10]

Due to possible high salinity of produced water, selecting the appropriate desalination technology is key to the development of a synergistic strategy. There is a wide variety of desalination technologies available, including thermal, membrane, and other types. This study examines membrane distillation, a cost-efficient method for desalination that can operate at low temperatures and utilize energy from waste heat, such as flared gas. This preliminary simulation of the membrane distillation process, constructed in both MATLAB and Aspen Plus, will examine effects of different operating variables, energy requirements, and a cost assessment. The ultimate objective is to provide a computational framework for the cost and energy requirements of the membrane distillation system.

2 Water management problem of hydraulic fracturing

2.1 Introduction

The development of unconventional natural gas resources in deep shale formations is a rapidly growing market. According to the Energy Information Administration, natural gas accounts for 21% of the fuel used to power electricity production and 24% of the total energy demand in the US. This dependence on natural gas is only expected to increase over the new few decades [7]. The exploration, development, and production of unconventional natural gas resources have greatly expanded to meet this growing demand. These unconventional sources include coal-bed methane, tight shale, and shale gas. The last of these is the fastest and most promising source of natural gas, projected to contribute the most to the natural gas production in the next two decades [8]. This growth in shale production can be largely attributed to the development of two techniques: hydraulic fracturing and horizontal drilling.

Hydraulic fracturing is the fracturing of rock in deep shale formations by highly pressurized hydraulic fluids and propping agents pumped into well bores to stimulate the flow of shale gas. The well drilling can extend vertically and then horizontally up to thousands of feet both ways [9]. After the well cycle has been completed, the injection pressure is reduced to permit gas and fluids to return to the surface through the borehole.

Despite hydraulic fracturing's promise of meeting the US's growing energy demands, there are a number of environmental complexities associated with this technology. One of these environmental issues is how to manage the sheer volume of water produced in the hydraulic process. As mentioned previously, produced water most generally refers to water already present in the formation while flowback water usually indicates the hydraulic fluids injected for the fracturing process. Management of these high volume waste waters, whether for treatment or disposal, is a major challenge in achieving profitability in the development of these shale gas reservoirs.

2.2 Flowback and produced water

The flowback period is typically 8-10 days after the fracturing is complete and the injection pressure has been reduced [2]. Flowback water refers to the fracturing fluid that returns to the surface within the flowback period and is heaviest the first day (approximately 1,000 m^3/day), diminishing over time [13]. The larger portion of this flowback water is injection fluid, while the rest is formation water, whose proportion will increase over time. Flowback water can include fracturing additives, clay, metals, chemical additives, dissolved metal ions and TDS as shown in Fig. 4. [8]. Additionally, drilling and producing requires an estimated

Parameter	Feed Water	Flowback
pH	8.5	4.5 to 6.5
Calcium (mg/l)	22	22,200
Magnesium (mg/l)	6	1,940
Sodium (mg/l)	57	32,300
Iron (mg/l)	4	539
Barium (mg/l)	0.22	228
Strontium (mg/l)	0.45	4,030
Manganese (mg/l)	1	4
Sulfate (mg/l)	5	32
Chloride (mg/l)	20	121,000
Methanol (mg/l)	Neglible	2,280
TOC (mg/l)	Neglible	5,690
TSS (mg/l)	Neglible	1,211

Figure 4: Water quality of flowback water in the Marcellus Shale [16]

2-4 million gallons of water (48,000-95,00 barrels) and the median water use for a developing shale gas well in Texas is 2.8-5.7 million gallons (67,000-140,000 barrels) [11].

Fig. 5. shows the exact amount of water consumed for drilling and fracturing, as well as the flowback water for different shale plays in the US. The amount of this consumed volume that is returned to the surface has been estimated to be around 8-15%, 10-40%, 9-53%, and 30-70% although exact compositions and volume depend heavily on the formation geography and as well as operating parameters during well development [10].

After the flowback period, the fluid returning from the well is generally referred to as produced water and flows at a much lower rate, approximately 2-8 m^3/day [2]. Produced water refers to the water that previously and naturally existed within the shale gas formations and is stimulated to flow to the well surface during the hydraulic fracturing process. Produced water can contain very high concentrations of total dissolved solids (TDS); dissolved and suspended organics, such as oil and grease; suspended solids, such as corrosion and scale

Shale	Gallons Used for Drilling	Gallons Used for Fracturing	Million Gallons Used per Well	Initial Volume of Water (flowback at first 10 days of production process)
Barnett	250,000	3,800,000	~ 4.0	0.4-0.6 Million Gallons (10%-15% of total water needed for fracturing a new well)
Haynesville	600,000	5,000,000	~ 5.6	0.25 Million Gallons (~5% of total water needed for fracturing a new well)
Fayetteville	65,000	49,000,000	~4.9	0.5-0.73 Million Gallons (10%-15% of total water needed for fracturing a new well)
Marcellus	85,000	5,500,000	~5.6	0.56-0.84 Million Gallons (10%-15% of total water needed for fracturing a new well)

Figure 5: Volume of water consumed for drilling and fracturing by shale plays [12].

products, bacteria; fracturing chemicals, such as proppants, friction reducers, biocides, and corrosion inhibitors; and naturally occurring radioactive material [2]. However, exact proportions are again dependent on the geography and geology of the formation. Additionally, the physical and chemical composition of flowback and produced waters vary greatly over the lifetime of a shale gas well [14]. Because of this, selection of a desalination technique can be tricky as it must be capable of combating these physicochemical changes as well as treat high-salinity waters.

Despite the vast variety of constituents of concern, the TDS concentration is most problematic and the primary consideration in discharge quality control for reuse [1]. For this reason, there is an entire spectrum of desalination options for treatment of flowback and produced water. Each technology has its individual advantages as well as operational and economic limitations [15]. Three of these desalination technologies show great potential for treatment of high-salinity shale gas produced water: mechanical vapor compression (MVC), forward osmosis (FO), and membrane distillation (MD). All three of these technologies can meet the TDS concentration limits on the permeate that is required for reuse and fit within the infrastructure constraints of many on-site shale gas treatment sites [10]. Additionally, the energy requirements and associated costs are competitive to the commercialized and currently established thermal treatment technologies. This study will focus on membrane distillation and is further discussed in the subsequent section.

3 Membrane distillation

3.1 History and resurgence of interest

Membrane distillation (MD) is an emerging technology for thermally driven separation processes that can utilize low-grade heat to drive mass transport through a hydrophobic, microporous membrane. This hydrophobic membrane allows pure vapor to separate from an aqueous feed stream through the membrane pores due to the surface tension forces. The aqueous feed stream must be in direct contact with one side of the membrane without penetrating and wetting the dry membrane pores [17]. The driving force of the separation is powered by the transmembrane vapor pressure differences activated by the temperature differences on either side of the membrane [18].

MD was first patented in 1963 with its first publication 4 years later in 1967 [19]. However, the promise of MD during this time was quickly overshadowed by the observed higher production capabilities of reverse osmosis. Not until the early 1980s did interest for MD in the academic and commercial communities return thanks to a number of advancements in the MD field that made it a more appealing desalination technique. These improvements included not only the development and availability of novel and less expensive membranes and modules, but also its capability of utilizing low-grade waste and alternative energy sources, such as solar, geothermal, and in this study, flared gas energy [20-22]. Today, MD has been investigated for application in desalination where the primary concern is removal of TDS from produced waters [23].

3.2 Process configuration

3.2.1 Four techniques

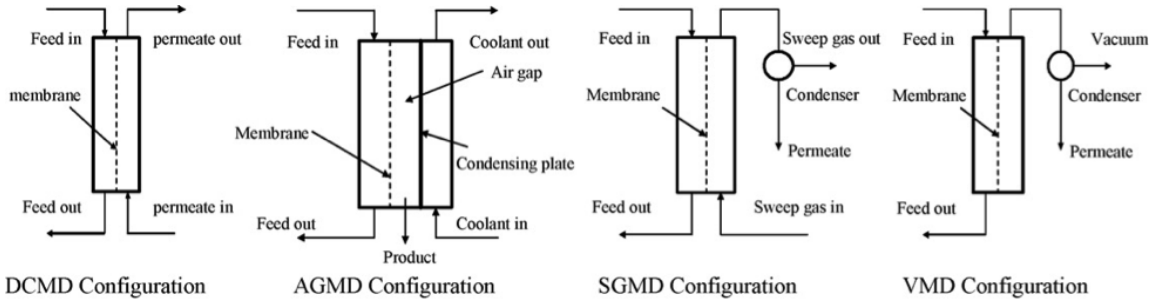

Figure 6: Different types of MD configurations [17]

There are four basic techniques of MD that primarily differ in the way the vapor pressure gradient is maintained [24-30]:

1. Direct contact membrane distillation (DCMD), the configuration used in this study, contains a countercurrent flow of cold and hot aqueous solution. The hot feed flows in direct contact with the permeate side of the membrane, only allowing the volatile molecules to cross the membrane and condense in the cooler permeate stream. The transmembrane vapor pressure difference is driven by the temperature differences. This is the most suitable method for non-volatile solutes in desalination applications.
2. Air gap membrane distillation (AGMD) configuration functions very similar to DCMD except for the presence of a stagnant air gap in between the membrane and the condensation plate. The volatile vapor molecules must cross both the membrane interface and air gap in order to condense over a cold surface.
3. Sweeping gas membrane distillation (SGMD) replaces the cold aqueous solution on the permeate side with a sweep of cold inert gas that carries the vapor molecule to outside the membrane module where condensation takes place.
4. Vacuum membrane distillation (VMD) uses a vacuum pump to apply a vacuum to the permeate side of the membrane module with lower pressure than the saturation pressure of the volatile molecules. For this configuration, condensation occurs outside of the membrane module.

3.2.2 Membrane characteristics

The return of interest in MD is partly thanks to the advancement of the membrane, which has become more available, reasonably priced, and optimal for the designated system since the 1960's [18]. Today, membranes are held to much higher standards and are expected to exemplify the following properties for optimal functionality [17, 18, 31, 32]:

1. *Thinness.* The permeate flux has been shown to be inversely proportional to the thickness of the membrane. As a result, the membrane should have a sufficient but not excessive thickness.
2. *Pore non-wettability.*
    - Small pore sizes. Pore sizes ranging from 10nm-1μm are recommended. When the aqueous solution is brought into contact with the membrane, the pores should be small enough to prevent penetration of aqueous molecules while allowing the penetration of vapor molecules.
    - High surface tension. High water contact angle, along with small pore sizes, helps membranes avoid pore wettability and contributes to high porosity for the

vapor phase.

- Low surface energy of membrane material. Membrane materials most commonly selected in MD are polytetrafluoroethylene (PTFE), polyvinylidenefluoride (PVDF), polyethylene (PE), and polypropylene (PP).

3. *Immunity to fouling.* Although fouling of membranes is still an issue for MD, it is much less common than for other conventional desalination technologies like reverse osmosis or ultrafiltration due to the relatively large pore sizes. Fig. 7 shows a conceptual illustration of a worst-case scenario in the DCMD membrane module. A) Temperature difference that result in transmembrane vapor pressure. B) Wetting of pores that diminish permeate mass flux. C) Fouling of membrane that further reduces permeate flux.

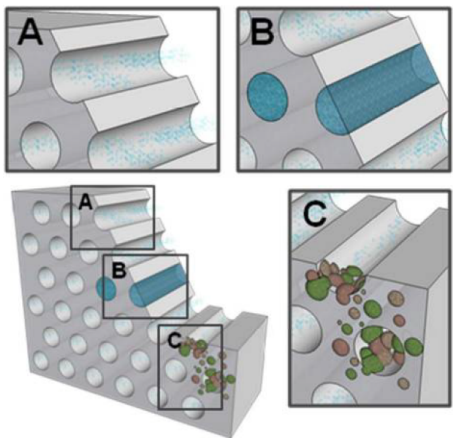

Figure 7: Conceptual illustration of worst-case scenario in DCMD [10].

3.2.3 Principal operating variables

MD performance is controlled by a number of different operating variables [10,33-34].

1. *Feed temperature.* MD flux is highly dependent on feed temperature, which can range from 40-90 C. The required energy can be harvested from low-grade waste heat. Furthermore, the vapor flux increases exponentially with an increase in feed temperature as described by the Antoine relation. As a result, the higher the feed inlet temperature, the greater the driving force and vapor flux, resulting in increased productivity.

2. *Feed inlet concentration.* MD is an especially promising desalination technique because it has the capability of treating highly concentrated solutions of TDS without suffering large permeate flux drops observed in other pressure driven processes. For

example, doubling the TDS concentration only reduces resultant permeate flux by 5%. Thus, MD is suited for desalinating high-salinity sources without incurring substantial productivity penalties.

3. *Temperature gradient.* Since the driving force in MD is the transmembrane vapor pressure, a lesser temperature gradient will yield a smaller permeate flux and thus a less effective process. Along these lines, a higher permeate temperature is likely to result in a smaller permeate flux due to the decrease in the transmembrane vapor pressure gradient.

3.2.4 Pre and post treatment

Although fouling propensity is lower in membrane distillation than for other membrane processes as discussed above, fouling can still occur and cause detrimental impacts to the process performance (Fig. 7). Fouling can clog membrane pores, resulting in significant decline in permeate flux and performance. Fouling can also result in pore wetting, which can disrupt heat and mass transfer [10]. Increased fouling can be anticipated as the TDS concentration of produced water grows with time.

Thus, pretreatment can be a powerful precautionary tool for fouling prevention. This procedure can include anything from early foulant removal, periodic membrane cleaning, to removal of components inclined to wet membrane pores [18]. A pre-filter is often used to screen out larger particles and remove any surfactants (like emulsifiers, wetting agents, or friction factors) still present in the stream to be treated. Alklaibi et al. has shown that pretreatment of raw water can increase permeate flux by 25% [18].

Post treatment may also be required for treated waters to meet specified water quality standards. These steps may include removal of volatile compounds, gasses, and other molecules that may have been transported to the permeate. Sometimes, remineralization and pH stabilization of the treated water via lime beds may be required to meet water quality standards [33].

3.3 Energy efficiency and water production cost

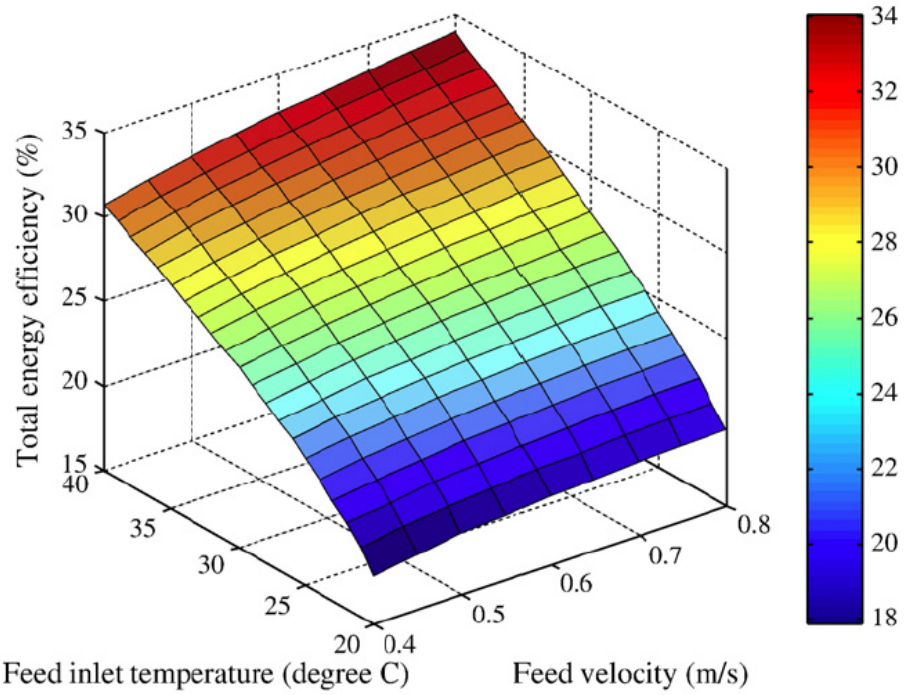

Figure 8: Effect of feed inlet temperature and velocity on total energy efficiency [41].

Literature has always found that low temperature DCMD models have encountered serious challenges with energy efficiency, which can be visualized in Fig. 8. A dynamic simulation of DCMD conducted by Bui et al. reveals that increasing feed inlet temperature and its velocity improves the DCMD performance while reducing operating time and energy consumption, resulting in overall improvement in energy efficiency [41].

An increase in feed inlet temperature, the driving force in membrane distillation, enhances the transmembrane permeate flux. Thus, as the temperature gradient increases, less membrane material is needed to match the same permeate flux. Less membrane results in less capital cost. Conversely, a higher temperature gradient requires more energy input, increasing the operation and maintenance costs [44]. Fig. 9 illustrates the optimization between the membrane and heating costs.

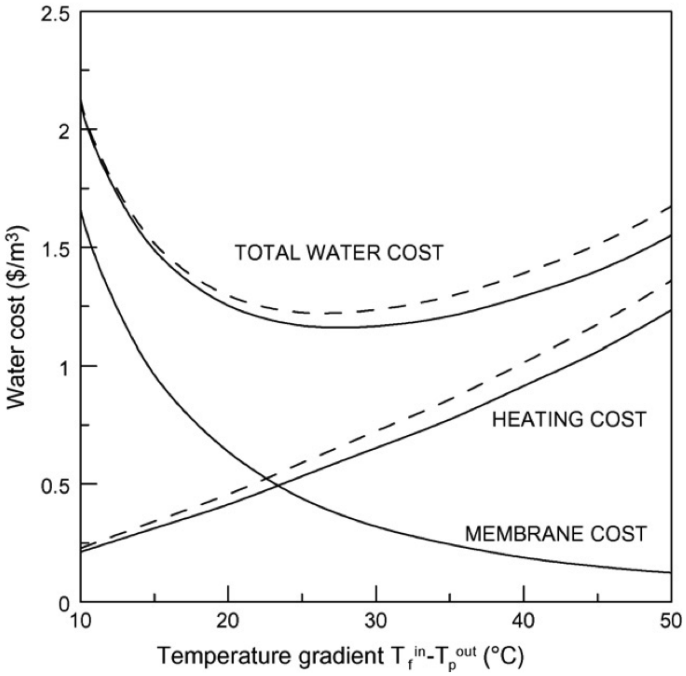

Figure 9: Water cost for DCMD as a function of temperature gradient [44].

Assuming fully developed MD technology, a total production cost for purified water production rate at 3,800 m^3/day has been estimated. A thorough economic analysis has been tabulated by Obaidani et al. which estimated that total water cost for MD is \$1.23/m^3 without heat recovery and \$1.17/m^3 with recovery heat [44]. Obaidani's estimates suggest that MD is economically competitive with reverse osmosis, whose water production cost estimate is \$1.26/m^3 [44]. Alklaibi et al. estimates the cost of MD produced water to be \$1.32/m^3 [18] while Banat et al. confirms the \$1.23/m^3 estimate by Alklaibi et al. [28].

4 Preliminary simulation of membrane distillation

The applicability of membrane distillation extends far and wide as a cost-efficient desalination method. MD can utilize waste heat to fuel its process and achieve a high solid content yield (up to 65% w/w even at extremely low operating temperatures like 25 C) [35]. However, a number of studies have shown that low-temperature MD process can encounter issues in energy inefficiency [36]. For this reason, reverse osmosis has attracted more interest over the past two decades, and there are currently no large-scale membrane distillation system in existence in commercial use [37].

Thus, there is a need to optimize the MD process to lower energy requirements while avoiding compromise with production and flux throughout operation. This optimization can be achieved using a variety of tools. In this study, the simulation has been first programmed in MATLAB to solve the heat and mass transfer system of a DCMD process and then also programmed in Aspen Plus, a commercial software package that can provide a powerful simulation platform for chemical engineering processes [37-38]. Aspen Plus can be very useful for studying the MD system for purposes of energy efficiency and economic analyses.

4.1 Simulation using MATLAB

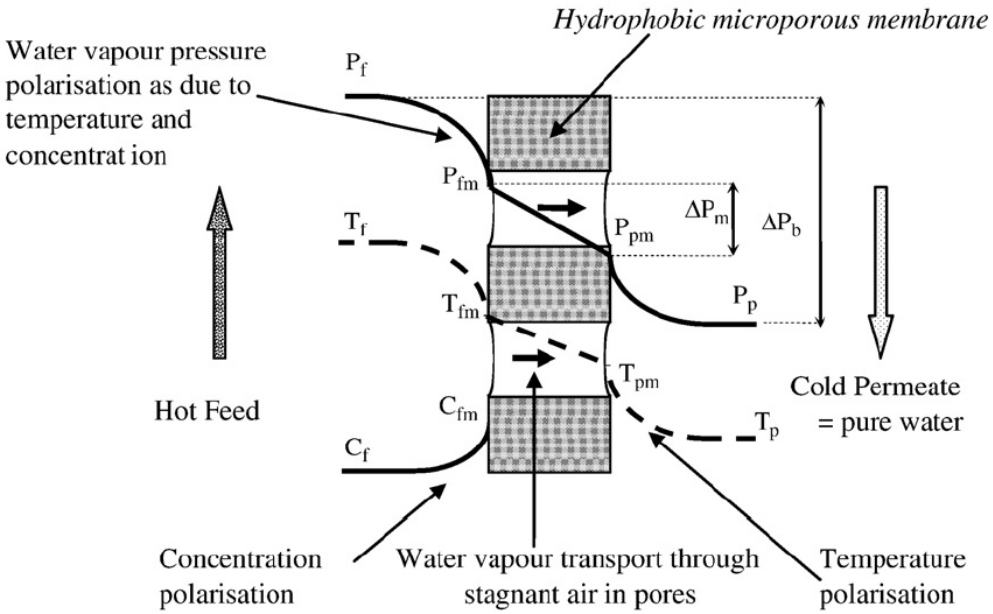

Figure 10: Cross-flow DCMD and associated polarization effects [39].

The simulation in MATLAB will provide a computational framework for solving the highly nonlinear heat and mass transfer system within a hollow fibre module (HFM) in a crossflow DCMD system. The HFM configuration consists of a bundle of hollow fibers housed within a heat exchanger. The result is a preliminary simulation of the membrane module, the core design element of the system, using MATLAB. Fig. 10. illustrates the driving force of the MD system as well as the temperature differences between the hot and cold streams. The temperature and resulting pressure gradients drive the transmembrane heat and mass transfers in the DCMD system.

Table 1. Characteristics of membrane module

Hollow fibre membrane module	
Length of the fibres, L (m)	0.5
Inner diameter of shell, d_i (mm)	0.33
Outer diameter of shell, d_o (mm)	0.63
Membrane thickness, δ (μm)	150
Packing density, ϕ (%)	60
Porosity, ϵ (%)	75
MD coefficient, C (kg/m^2*h*kPa)	8.6E-7
Membrane material	polypropylene

The basic characteristics of the membrane module and operating parameters used in the simulation are listed in the table above.

4.1.1 Heat and mass transfer theory

Fig. 11 shows an example control volume of differential length for a DCMD module, illustrating how the theoretical heat balances depend on the inlet and outlet temperatures of both the feed and permeate. Q^F represents heat released by feed; Q^P, heat gained by permeate; Q_m, heat transferred across membrane; T_{pi}, T_{po}, permeate inlet and outlet temperature; T_{fi}, T_{fo}, feed inlet and outlet temperatures. These heat fluxes are generally maintained as constant over the membrane length and are related by Eq. (1) and illustrated in Fig. 11. The amount of heat lost by the feed side, Q^F, and gained by the permeate, Q^P, can be defined by Eqs. (2) and (3).

$$Q^F = Q^P = Q_m \tag{1}$$

$$Q^F = m_f C_f (T_{fi} - T_{fo}) \tag{2}$$

$$Q^P = m_p C_p (T_{po} - T_{pi}) \tag{3}$$

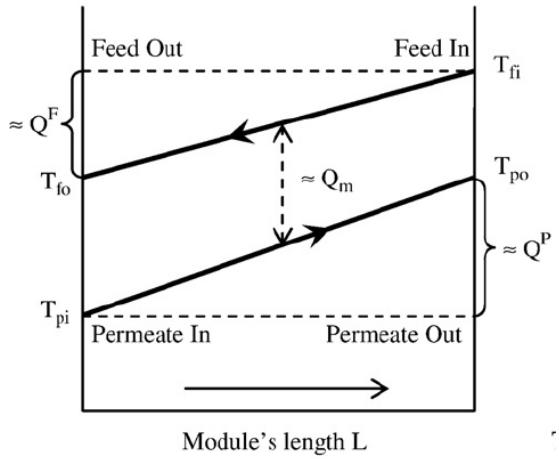

Figure 11: Theoretical heat balance along length of membrane module [39].

The mass flow rates, m_{f} and m_{p}, in Eqs. (2) and (3) were calculated by using velocity and density of the brine feed and pure permeate water respectively, as recommended by literature [40].

The transmembrane heat flux, $\mathrm{Q_m}$, is comprised of two components: the latent heat released by diffusing water vapor across the membrane, $\mathrm{Q_{vapor}}$, and the conductive heat through the membrane matrix, $\mathrm{Q_{cond}}$, as demonstrated in Eq. (4). This transmembrane heat flux is equal to the convective heat flux flowing through both the feed, $\mathrm{Q_f}$, and permeate, $\mathrm{Q_p}$, boundary layers as defined by Eqs. (5-7).

$$Q_m = Q_{vapor} + Q_{cond} = A_i h_m (T_{fm} - T_{pm}) + A_i J \Delta H_v \tag{4}$$

$$Q_f = A_o h_f (T_f - T_{fm}) \tag{5}$$

$$Q_p = A_i h_p (T_{pm} - T_p) \tag{6}$$

$$Q_f = Q_p = Q_m \tag{7}$$

The thermal conductivity of the membrane matrix, $\mathrm{h_m}$, can be approximated using a theoretical model or a regression analysis of experimental data [39]. The heat transfer coefficients, $\mathrm{h_f}$ and $\mathrm{h_p}$, in the feed and permeate boundary layers can be described in a number of ways. One relatively straight-forward and widely adopted method [40] is shown in Eqs.

(8-10) where the hydrodynamic Nusselt Number (Nu) is related to the Reynolds Number (Re) and temperature-dependent Prandtl number (Pr).

$$Nu_f = \frac{h_f d_i}{k_m} = 1.662[Re_f Pr_f \frac{d_i}{L}]^{0.33} \tag{8}$$

$$Nu_p = \frac{h_p d_o}{k_m} = 0.206(Pr_p)^{0.36} \tag{9}$$

$$Re_{f,p} = \frac{d_{i,o} u_{f,p} \rho_f}{\mu_f}; Pr_{f,p} = \frac{C_{f,p} \mu_{f,p}}{k_m} \tag{10}$$

In DCMD, the vapor pressure difference resulting from the temperature difference between the two streams is the driving force for the transmembrane water vapor transfer. The mass flux is only dependent on the heat transfer rather than the molecular diffusion law. A number of mathematic models such as Knudsen, Poiseuille and molecular diffusion models have been employed to calculate mass flux [40]. For this study, a widely accepted empirical model for water flux across the membrane is used and demonstrated in Eq. (11) [41]. The water vapor pressures at the membrane surface, P_{fm} and P_{pm}, can be calculated using the Antoine's equation in Eq. (12).

$$J = C(P_{fm} - P_{pm}) \tag{11}$$

$$P_{fm,pm} = exp(23.20 - \frac{3816.44}{T_{fm,pm} - 46.13}) \tag{12}$$

The MD coefficient, C, or the membrane vapor permeability is dependent on the physical properties of the membrane matrix, such as tortuiosity, porosity and diffusivity of water vapor [42]. The value for C in this study is considered relatively constant and suggest that C is only slightly dependent on temperature.

4.1.2 Problem-solving methodology

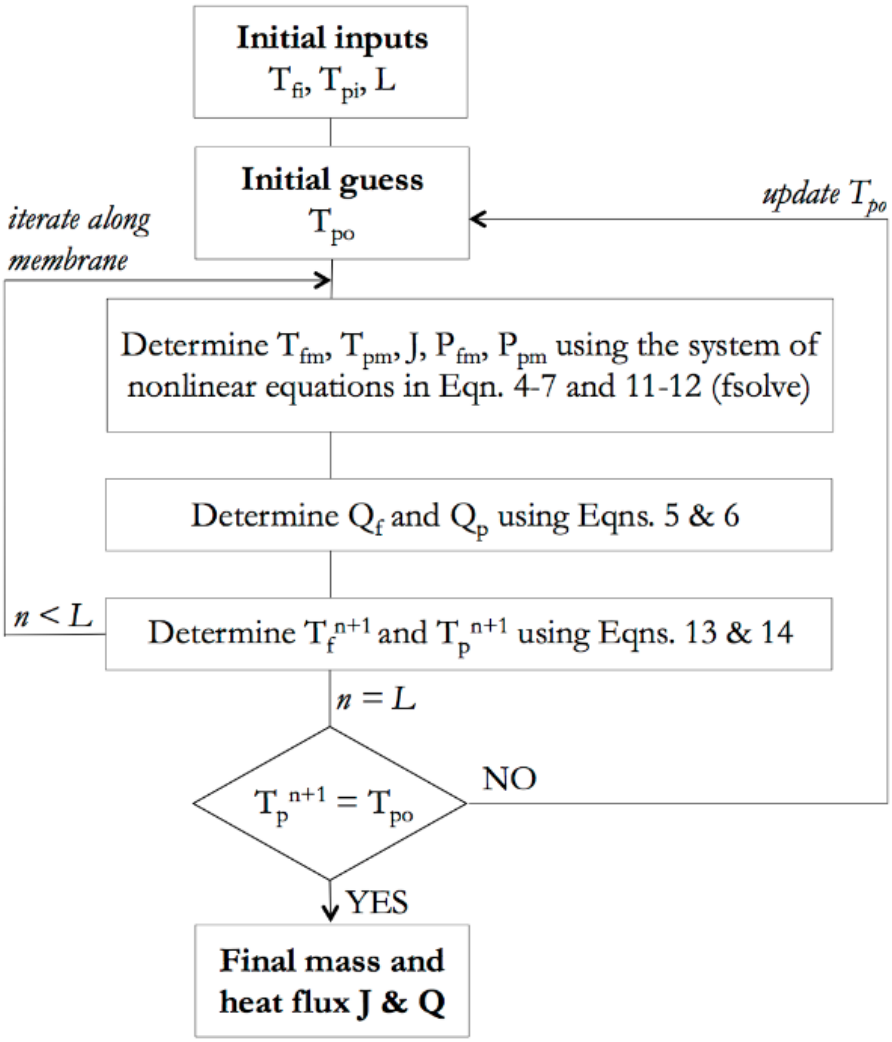

Figure 12: Algorithm for steady-state simulation of DCMD in a HFM.

The double-loop iterative MATLAB algorithm developed for the DCMD simulation in this study is shown above in Fig. 12. The heat and mass transfer processes in the DCMD model are dependent on the physical properties of the feed and permeate streams. Thus, a guess for the outlet temperature for the permeate stream is selected for the first iteration loop (although outlet temperature of the feed stream would also work). This guess is illustrated in Fig. 13. as T_{po} and is incrementally updated from right to left until it reaches T_p^L. A

nonlinear system of equations using Eqs. (4-7,11,12) can be constructed to solve for the temperature of the feed and permeate stream at the membrane, T_{fm}, T_{pm}; mass flux, J; and the pressure of the feed and permeate stream at the membrane, P_{fm}, P_{pm}. The inputs to this system of equations are the initial guess, T_{po}; the known inlet transmembrane temperature difference, T_{fi}-T_{pi}; and the length of the membrane fibre tube, L. The nonlinear system was solved in MATLAB using the *fsolve* function.

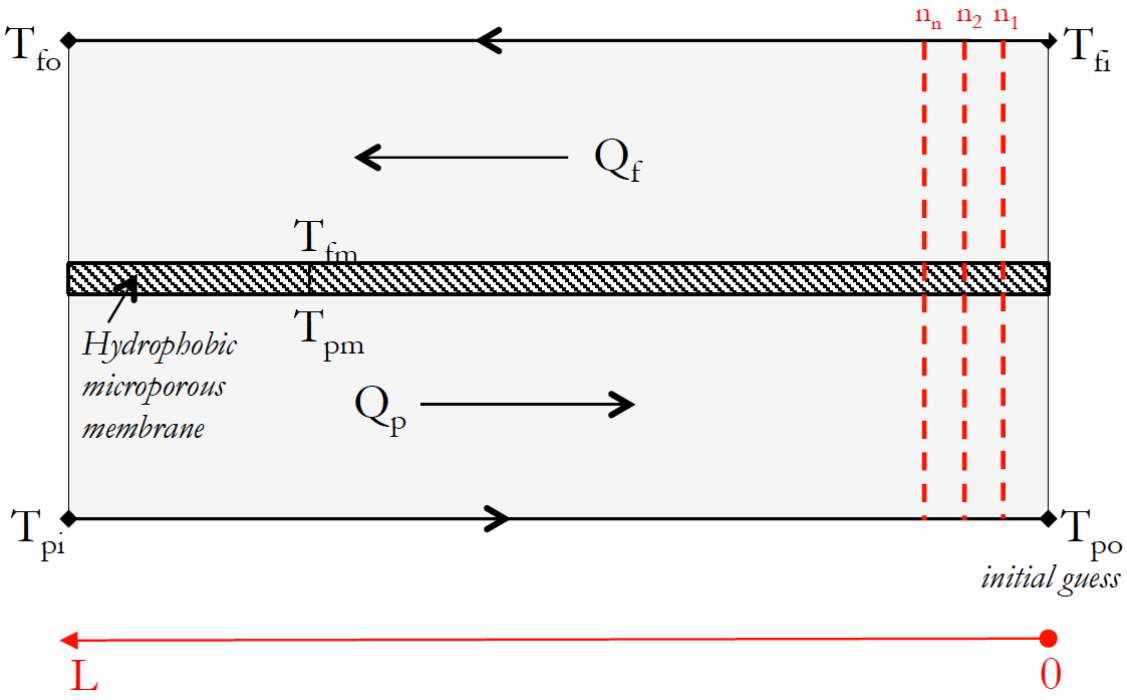

Figure 13: Heat fluxes for steady-state simulation of DCMD across the length of a membrane module.

$$\frac{T_f^{n+1} - T_f^n}{\Delta z} = \frac{Q^n 2\pi r}{m_f C_p} \tag{13}$$

$$\frac{T_p^{n+1} - T_p^n}{\Delta z} = \frac{Q^n 2\pi r}{m_p C_p} \tag{14}$$

Using these parameters, the amount of heat transferred at each increment, n, between the two streams (Q_f, Q_p) can be determined using Eqs. (5) and (6) and subsequently fed into the inner loop to find the temperatures of the feed and permeate at the next increment (T_f^{n+1}, T_p^{n+1}) along the membrane module as shown by the dotted red lines (n_{n+1}) in Fig.

13. The temperature of the feed and permeate at the next step, (n+1), can be calculated by Eqs. (13) and (14), modified from Eqs. (2) and (3). T_f and T_p are iterated within the inner loop along the entire length of the membrane, L.

After iteration of the inner loop is complete, the temperature of the permeate at the inlet, T_p^L, is compared to the previously designated permeate inlet temperature, T_{pi}. If they are unequal, the initial guess for the permeate outlet, T_{po}, is updated and iterated over the first loop again. In this simulation, in order to avoid missed temperatures, the initial guess was set to an impossibly low value and increased over iterations. If T_p^L is equal to T_{pi}, the guess for T_{po} is sound and the final mass and heat fluxes can be extracted from the simulation.

4.1.3 Energy analysis

The total energy of the system is broken up into two components: energy consumed by the feed stream and the energy needed for circulation of the two streams. The energy needed for circulation is a function of the fluid mass flow rates, viscosity and the flow geometry and is based on the assumption that the pressure lost due to the fiber matrix is about 15% [41]. The energy efficiency relation is a function of the total energy consumed in the system, matrix geometry, transmembrane flux, and heat of vaporization. These values can be calculated using Eqs. (15-17) [41]:

$$E_{DCMD} = \int_0^{T_f} (Q_f + Q_{circulation})dt \tag{15}$$

$$Q_{circulation} = \sum_{f,p} Q_{circulation}^{f,p} = \sum_{f,p} m_{f,p}(1 + 0.15)\Delta P_{f,p} \tag{16}$$

$$EE_{DCMD} = \frac{A_i \int_0^T J(t)\delta H_v(t)dt}{E_{DCMD}} \tag{17}$$

4.2 Simulation using Aspen Plus

4.2.1 Flowsheet construction

Aspen Plus is a commercial software with a widely used simulation platform in chemical engineering processes. This software has recently been used to study the MD system. Since the feed stream is designated as a 5% brine cocktail, the thermodynamic model in Aspen Plus for electrolytes, NRTL-RT, was selected for use in the multistage simulation. In previous studies, the customized membrane module was first programmed using FORTRAN or MATLAB and then incorporated as a user-defined unit into Aspen Plus [37,38].

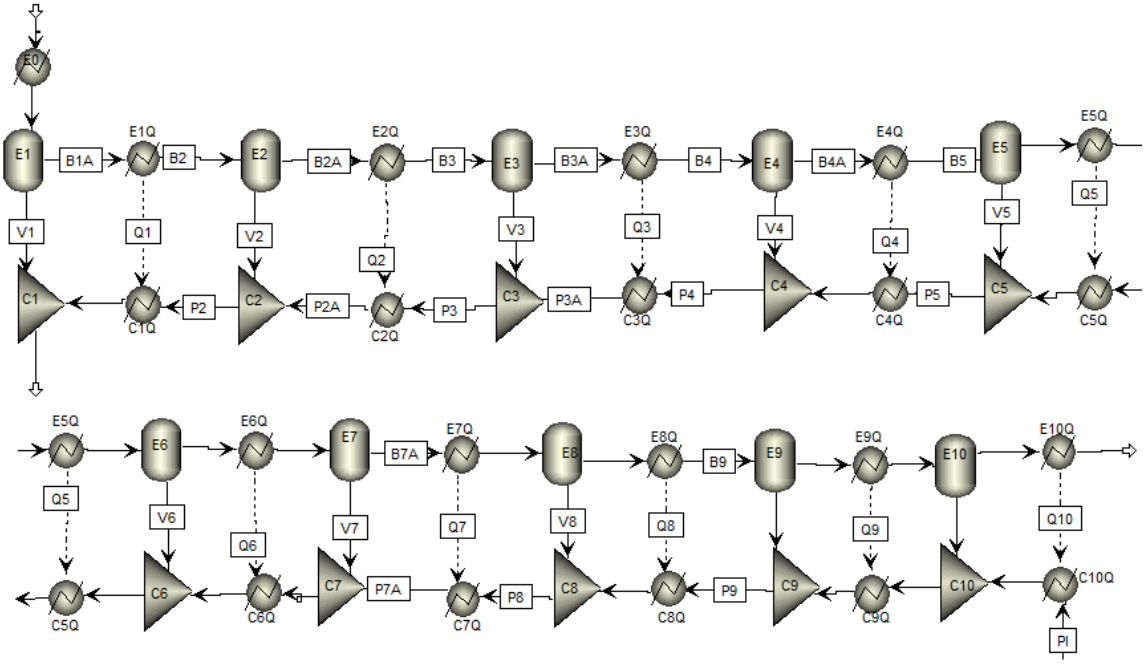

Figure 14: Entire 10-stage MD flowsheet.

In this study, an MD model using the flowsheet capabilities of Aspen Plus was constructed. The multistage operation is characterized by 10 stages and composed of a series of feed flash-evaporation blocks running up and absorption blocks running down. Fig. 14. illustrates the entire MD flowsheet in two rows with blocks E5Q and C5Q repeated to show continuity. For each stage, the mass transfer in the steam vapor is represented by a material stream, while the heat transfer from the flash-evaporation side to the absorption side can be represented by a heat stream. The heat and mass transfer is characterized by the FORTRAN calculator block, which has access to the necessary process variables in the flash-evaporation and absorption block to perform the necessary calculations.

Fig. 15. shows the first 2-stages of the 10-stage flowsheet. Each stage is represented by four blocks. For stage 1, a flash-evaporator (E1) and mixer (C1) characterize the mass transfer and its enthalpy from the brine feed to the permeate product stream. The heaters (E1Q and C1Q) characterize the transmembrane heat transfer. This series of 4 blocks is repeated 10 times to create the entire multistage operation. The calculator block embedded with the heat and mass transfer equations are specified as shown in Fig. 16.

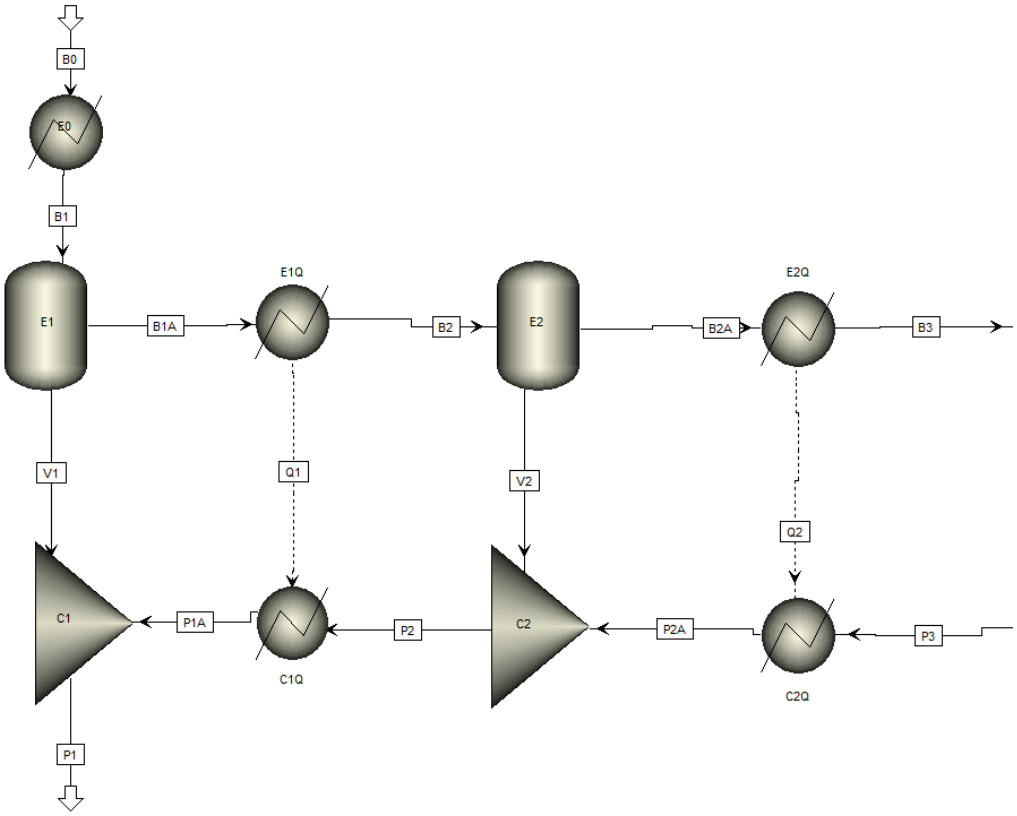

Figure 15: Two-stages of the 10-stage MD flowsheet.

The flash evaporator takes the saturated liquid brine (B1) and "flashes" the stream into a pure vapor (V1) and a residual liquid (B1A), which is more concentrated with NaCl than the feed (B1). The flash evaporators are configured to bring the streams to a pressure of -0.04 bar to create the pressure reduction necessary for the flash to occur. As the residual liquid stream (B1A -> B2 -> B2A) progress down the flash-evaporation blocks, heat is transferred (Q1) to the permeate stream and the temperature decreases along the stages. On the other hand, the vapor streams (V1) are condensed with the ongoing permeate stream (P2A -> P2 -> P1A) by the mixer (C1).

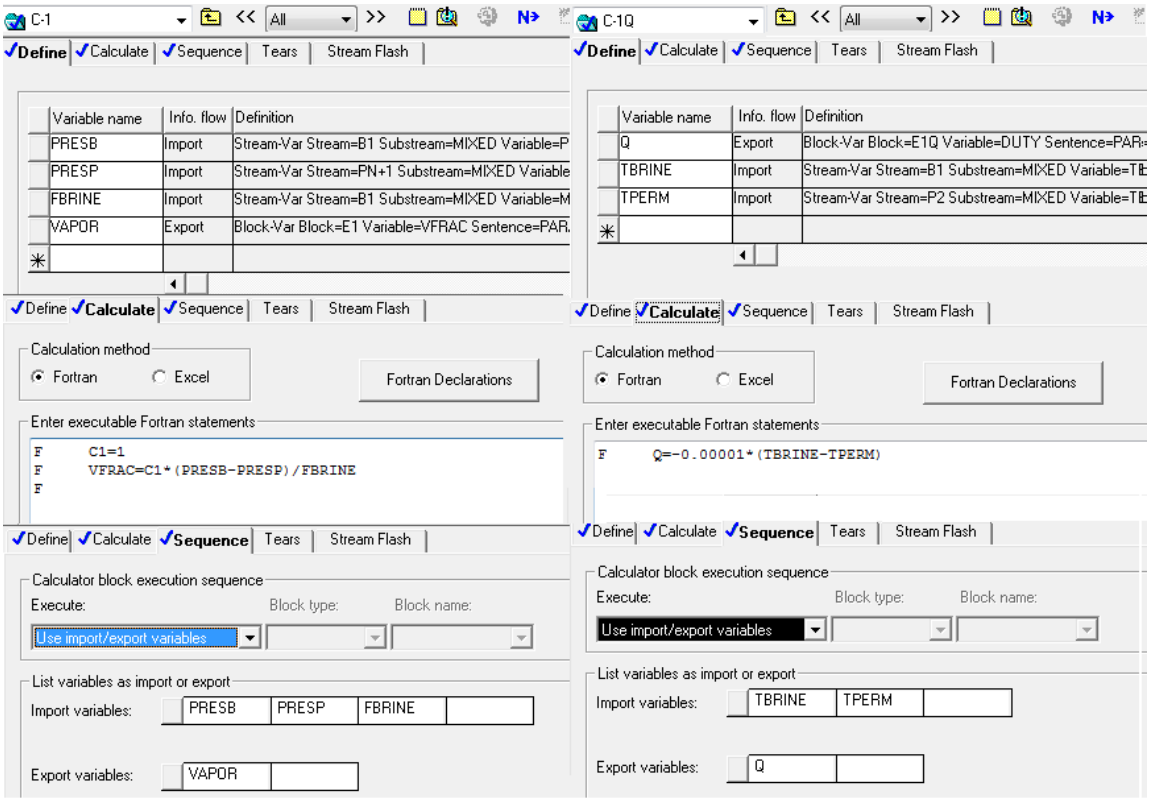

Figure 16: Heat and mass transfer equations.

To run the system, two variables of inlet feed and inlet permeate were specified. As shown in Fig. 16., the temperature and pressure of the feed inlet brine stream were selected to be 80 C and 1 bar, respectively. The brine inlet is composed of water and approximately 5% sodium chloride, as suggested by literature for produced water composition [10]. The temperature and pressure of the permeate inlet stream were selected to be 60 C and 0.3 bar, respectively. The permeate stream is pure, and often times, recycled from within this process.

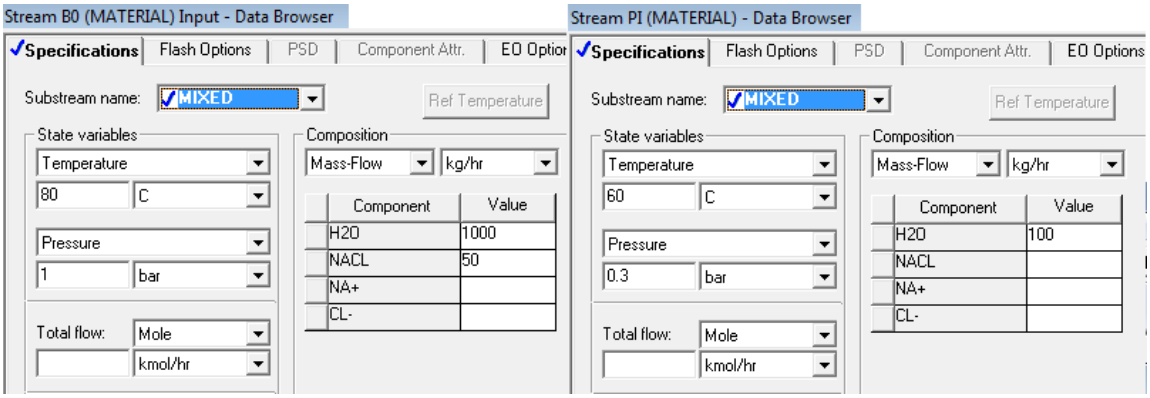

Figure 17: Specifications of the input streams.

4.2.2 Recovery ratio

The recovery ratio (RR), a system performance indicator, was calculated by dividing the permeate flow rate, m_p, by the feed flow rate, m_f (Eq. 18). A high recovery ratio indicates a relatively high permeate flow rate for a given feed flow rate. The expected recovery ratio from reported solar powered membrane distillation systems ranged from 1-4.5% [43].

$$RR = \frac{m_p}{m_f} * 100(\%) \tag{18}$$

5 Preliminary results of DCMD simulation

The DCMD module was examined as a function of membrane fiber length and feed temperature. The permeate inlet temperature was maintained for each iteration at 290 K and is not considered an operational variable in the simulation. The variation in feed and permeate temperature throughout the simulation can be used to perform additional energy efficiency and water production cost analysis.

5.1 Results using MATLAB

5.1.1 Spatial variations

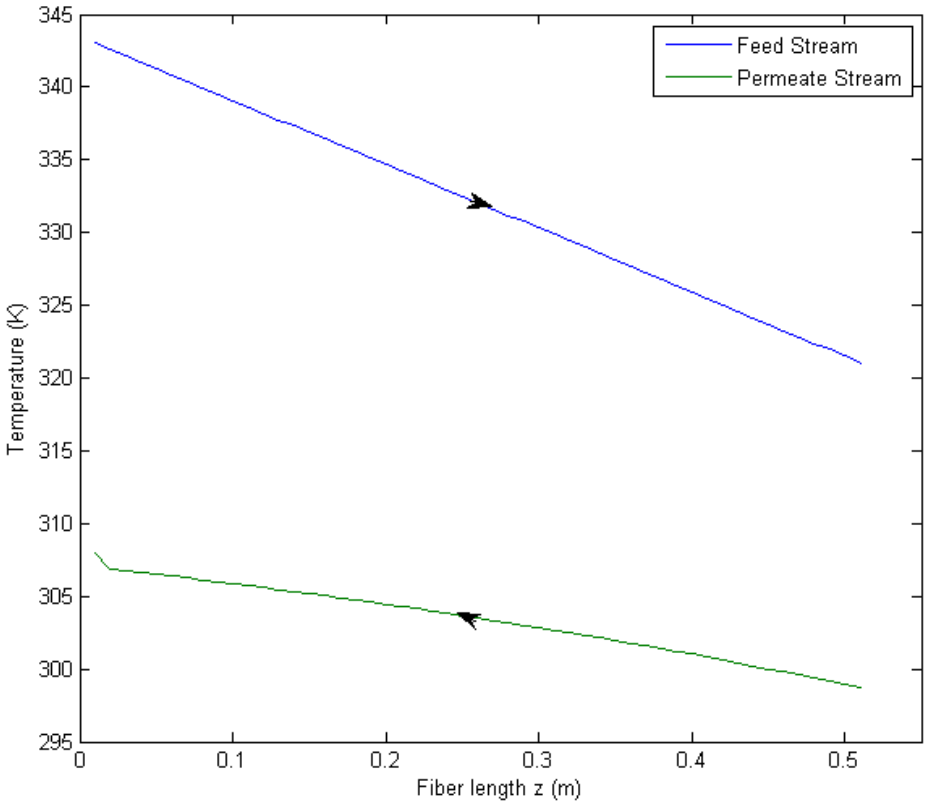

Figure 18: Temperature of feed and permeate as a function of membrane fiber length.

The variations of T_f and T_p as a function of the fiber length within the first iteration loop of the simulation are shown in Fig. 18. In this example iteration, the feed and permeate inlet temperatures were selected to be 343 K and 298 K, respectively. The feed temperature decreases linearly along the membrane length from 343 K to 323 K, losing heat. Conversely, the permeate side gains 18 K of heat. Due to the countercurrent flow pattern, the transmembrane temperature difference should remain approximately constant across the membrane length. The variability within the transmembrane temperature difference may be attributed to the difference in mass flow rates of feed and permeate.

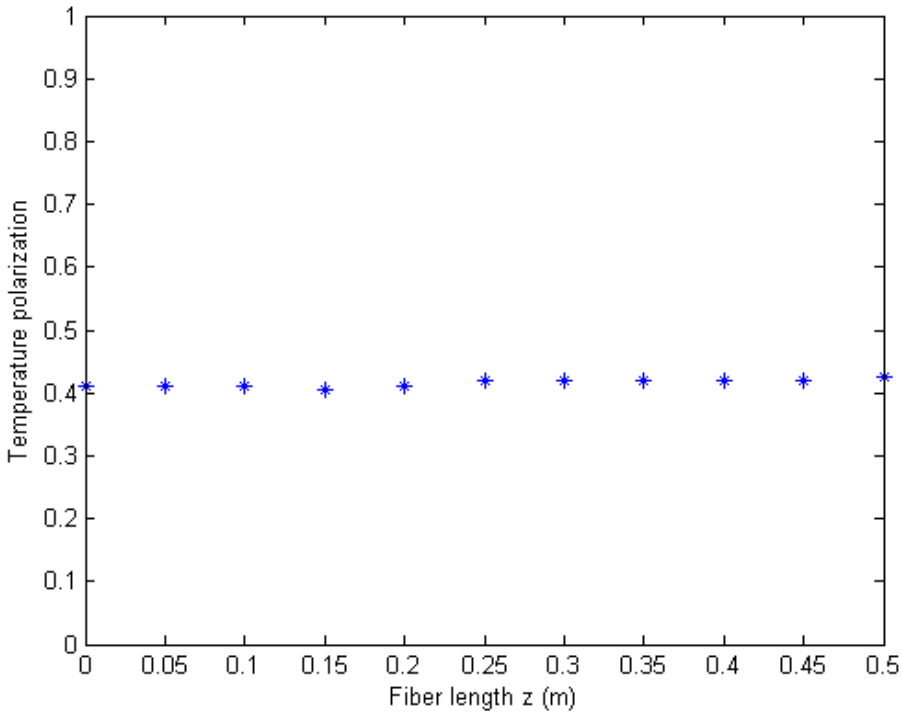

Figure 19: Temperature polarization as a function of membrane fiber length.

Fig. 19. illustrates the nearly constant temperature polarization across the membrane fiber length. The slight increase on the right may be a result of the variability in transmembrane temperature differences seen in Fig. 18. The temperature polarization coefficient can be calculated by $(T_{fm}\text{-}T_{pm})/(T_f\text{-}T_p)$, which implies that the transmembrane temperature difference is very similar to the temperature differences between the boundary layers of the feed and permeate. The temperature polarization, although slight, is mostly likely a result of smaller flow rates on the feed and permeate sides given that increasing velocity on either side will result in a smaller difference between bulk and membrane temperature.

5.1.2 Effect of feed temperature on transmembrane flux

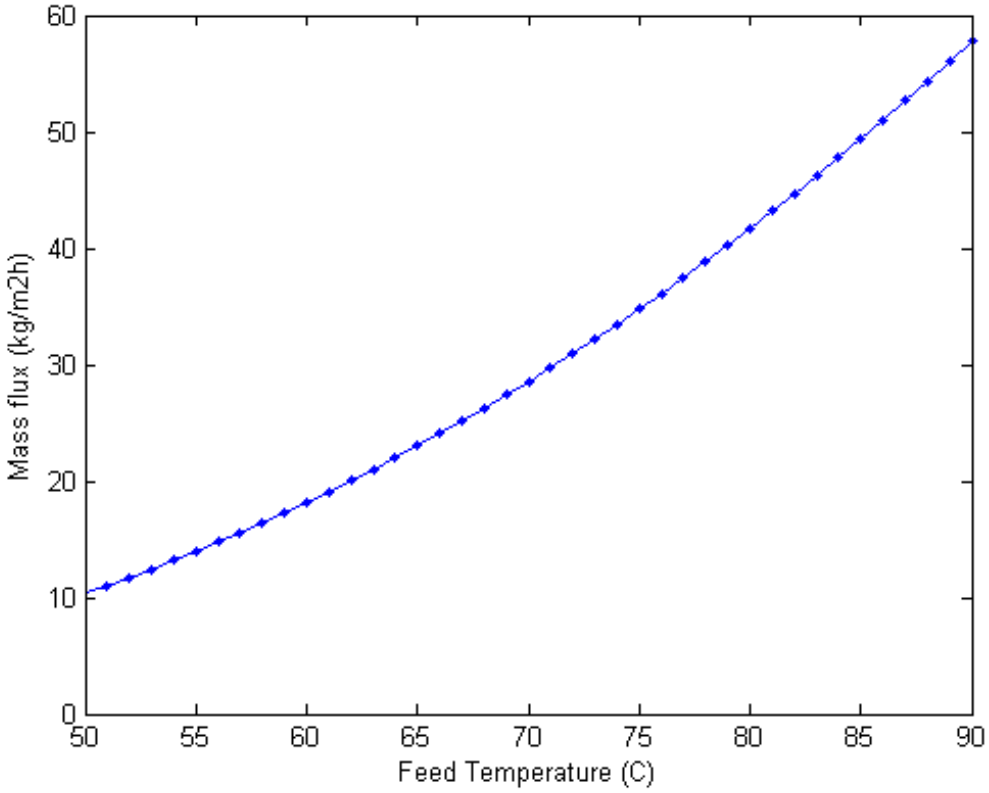

Figure 20: Mass flux as a function of feed inlet temperature.

Fig. 20. depicts the transmembrane mass flux as a function of feed inlet temperature ranging from 50 to 90 C based on the DCMD cross-flow simulation. As predicted, the permeate flux, an indicator of process performance, increases as the feed temperature is increased. Since a higher feed temperature also results in higher energy costs, a balance between cost and production must be sought. These results were compared to experimental data under the same conditions and found to be similar [42], suggesting that the MD module is an adequate predictor of MD module performance.

5.2 Results using Aspen Plus

The Aspen Plus simulation presented in this study demonstrates a preliminary operation. Future work on this simulation will involve more thorough investigation and include analyses on energy efficiency and water production cost as has been found in literature. Additionally, the simulated MD results obtained from the model need to be compared to experimental results from literature.

5.2.1 Variation of flow rate

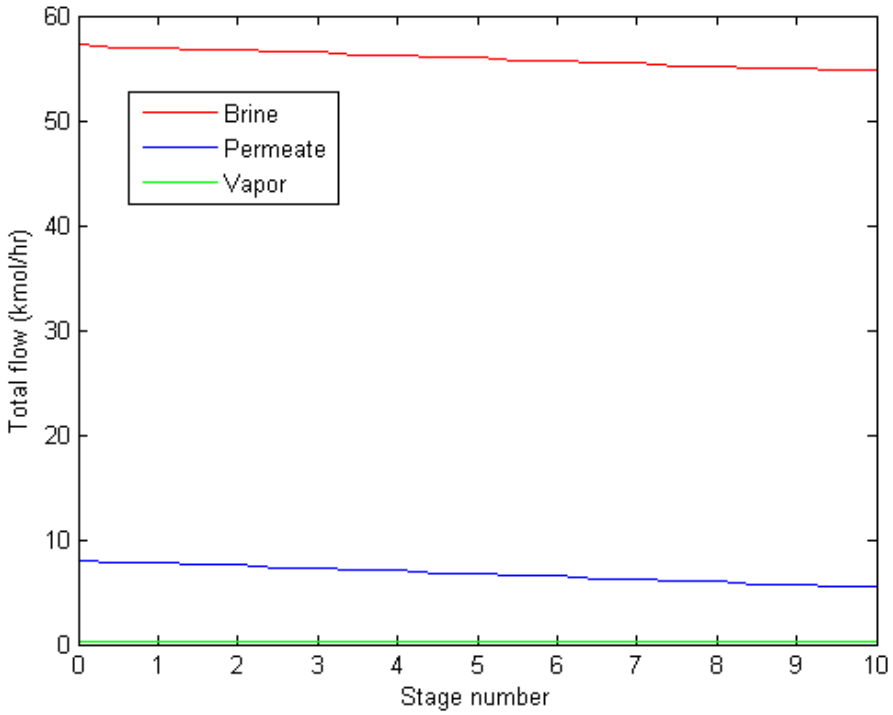

Figure 21: Flow rates of brine, permeate, and vapor streams along membrane.

Fig. 21. illustrates the variation in the flow rates of the feed, permeate and vapor streams along the multistage operation. The total flow of the brine feed diminishes slightly as the stream moves from stage to stage, while the total flow of the permeate stream increases the same amount as it moves from the final stage to the initial stage.

5.2.2 Recovery ratio

Performance indicators of solar powered membrane distillation systems.

System	Gran Canaria, Spain (compact system)	Gran Canaria, Spain (two-loop system)	Alexandria, Egypt	Irbid, Jordan	Aqaba, Jordan	Freiburg, Germany	Hangzhou, South China
Recovery ratio (%)	1–3.5*	4–5*	0.5–2*	4–4.5*	2–5	3.5–6.5*	0.25–1.5*
Performance ratio (kg/MJ)	0.1–0.85*	N/A	0.3–1.5*	N/A	0.2–0.3	N/A	N/A
GOR	3–6	3–6	0.97*	0.3–0.9	0.4–0.7	2–3.1*	0.85*
Thermal energy consumption (kWh/m^3)	N/A	180–260	N/A	200–300	200–300	N/A	7850

Figure 22: Performance indicators of solar-powered membrane distillation [44].

The preliminary results found that the recovery ratio, a system performance indicator, was 4.1% which lies in the upper range of recovery ratios obtained from single stage membrane distillation systems previously tested in literature [43]. This recovery ratio indicates a higher conversion of brine feed to permeate waters. This recovery ratio is relatively high compared to reported recovery ratio of solar powered membrane distillation systems that ranged from 1-4.5%, as seen in Fig. 22.

6 Conclusion

A computational framework for simulating a counter-current DCMD process in a hollow fibre configuration was developed and optimized in MATLAB. The steady-state simulation was verified through examination of the countercurrent spatial and temporal variations of the feed and permeate streams. Comparison to experimental data under the same conditions suggest that the MD module is an adequate predictor of MD performance. The simulation also found that the DCMD module was most effective, yielding the greatest transmembrane mass flux, when operating at a high feed inlet temperature.

A preliminary flowsheet simulation of a multistage MD operation was constructed in Aspen Plus, a widely used simulation platform in chemical engineering processes. The multistage operation is characterized by 10 stages and composed of a series of feed flash-evaporation and absorption blocks. The heat and mass transfer is characterized by the FORTRAN calculator block. The recovery ratio, a system performance indicator, was found to be 4.1%, reasonably high as compared to ratios found in literature, indicating a high rate of conversion of feed to permeate waters.

The work in this study is merely a preliminary glance into a much broader subject. Future avenues for exploration will include expansion of the Aspen Plus multistage flowsheet, optimization of energy efficiency, and investigation of associated water production costs.

Nomenclature

ϵ	membrane porosity, %
η	thermal efficiency of DCMD module
μ	viscosity of fluid, Pa s^{-1}
ψ	module packing density, %
ρ	liquid density, kg/m^3
τ	membrane tortuosity
$A_{i,o}$	internal, external surface area of hollow fibers, m^2
C	membrane distillation coefficient, kg m^{-2} h^{-1} kPa^{-1}
$C1$	mixer block
$C1Q$	heater block
C_p	specific heat capacity of material, J kg^{-1} K^{-1}
$d_{i,o}$	internal, external diameter of hollow fibers
$E1$	flash-evaporation block
$E1Q$	heater block
E_{DCMD}	total energy of DCMD, J
EE_{DCMD}	total energy efficiency of DCMD, %
$h_{f,p}$	boundary heat transfer coefficient on feed or permeate side, W m^{-2} K^{-1}
h_m	heat transfer coefficient of the membrane, W m^{-2} K^{-1}
J	mass flux, kg m^{-2} s^{-1}
L	length of hollow fibre, m
$m_{f,p}$	mass flow rate of the feed or permeate stream, kg s^{-1}
Nu	Nusselt number
$P_{fm,pm}$	water vapor pressure at membrane on feed or permeate side, Pa
Pr	Prandtl number
$Q^{F,P}$	heat flux gained or lost by the feed or permeate stream, W
Q_{cir}	heat required for circulation, W m^{-2}

Q_{cond} heat flux due to conduction, W m^{-2}

$Q_{f,p}$ heat flux across the feed or permeate domain, W

Q_m transmembrane heat flux, W m^{-2}

Q_{vapor} heat flux due to latent heat, W m^{-2}

Re Reynolds number

$T_{fi,pi}$ temperature of inlet feed or permeate stream, K

$T_{fi,po}$ temperature of outlet feed or permeate stream, K

$T_{fm,pm}$ temperature at membrane on feed or permeate side, K

7 References

[1] Fakhru'l-Razi A., et al., Review of technologies for oil and gas produced water treatment. J Hazard Mater, 2009. 170: p. 530-551.

[2] Gregory K. B., Vidic R.D., Dzombak D. A., ÒWater management challenges associated with the production of shale gas by hydraulic fracturingÓ, Elements, 2011 June 2011 v. 7 no. 3 p. 181-186.

[3] A. Kayode Coker (2007). Ludwig's Applied Process Design for Chemical And Petrochemical Plants, Volume 1 (4th ed ed.). Gulf Professional Publishing. pp. 732Ð737.

[4] Fielden S. (2013). ÒThe fight to limit Bakken shale flaring.Ó Oil and Gas Financial Journal. RBN Energy. http://www.ogfj.com/articles/2013/05/the-fight-to-limit-bakken-shale-flaring-.html

[5] Yoxtheimer D. (2012). ÒFlowback Management Trends and Strategies.Ó Exploring the Environmental Effects of Shale Gas Development in the Chesapeake Bay Watershed: Chesapeake Bay Scientific and Technical Advisory Committee.

[6] McCurdy R. (2012). ÒUnderground Injection Wells for Produced Water Disposal.Ó Chemicals and Water Reclamation. Chesapeake Energy Corporation.

[7] U.S. Energy Information Administration (EIA), ÒUS Energy Related CO2 Emissions in Early 2012 Lowest Since 1992Ó, Today In Energy, Available at: http://www.eia.gov/todayinenergy/detail.cfm?id=7350

[8] ÒPlan to Study the Potential Impacts of Hydraulic Fracturing on Drinking Water ResourcesÓ, Office of Research and Development, November 2011.

[9] Charlez, Philippe A. (1997). Rock Mechanics: Petroleum Applications. Paris: Editions Technip. p. 239. ISBN 9782710805861. Retrieved 2012-05-14.

[10] D.L. Shaffer, et al., Desalination and reuse of high-salinity shale gas produced water: Drivers, technologies, and future directions, Environmental Science Technology (2013) Just accepted*

[11] Murray, K.E., State-Scale Perspective on Water Use and Production Associated with Oil and Gas Operations, Oklahoma, U.S. Environmental Science and Technology. 2013.

[12] Roxana Darvari (2013)

[13] ALL Consulting and Groundwater Protection Council (GWPC), April 2009, ÒModern Shale Gas Development in the United States: A PrimerÓ, Prepared for US Department of Energy Office of Fossil Energy and National Energy Technology Laboratory

[14] Holditch S.A., ÒGetting the gas out of the groundÓ, Chemical Engineering Progress Journal (CEP) August 2012.

[15] King G.E., ÒHydraulic Fracturing 101: What every[one] should know about estimating frac risk and improving frac performance in unconventional gas and oil wells.Ó SPE Hydraulic Fracturing Technology Conference, February 2012.

[16] Kimbal B. (CDM), ÒKey Considerations for Frac Flowback/Produced Water Reuse and TreatmentÓ, NJWEA Annual Conference, 2011.

[17] M.S. El-Bourawi, et al., A framework for better understanding membrane distillation separation process, Journal of Membrane Science 285 (1-2) (2006) 4-29.

[18] A.M. Alklaibi, N. Lior, Membrane-distillation desalination: Status and potential, Desalination 171 (2) (2005) 111-131.

[19] B.R. Bodell, Silicone rubber vapor diffusion in saline water distillation, United States Patent no. 285,032 (1963).

[20] D.W. Gore, Gore-Tex membrane distillation, in: Proceedings of the 10th Annual Convention of theWater Supply Improvement Assoc, Hononulu, USA, 1982.

[21] S.I. Anderson, N. Kjellander, B. Rodesjo, Design and field tests of a new membrane distillation desalination process, Desalination 56 (1985) 345Ð354.

[22] K. Schnieder, T.J. van Gassel, Membrane distillation, Chem. Eng. Technol. 56 (1984) 514Ð521.

[23] A.K. Manna, M. Sen, A.R. Martin, P. Pal, Removal of arsenic from contaminated groundwater by solar-driven membrane distillation, Environ. Pollut. 158 (3) (2010) 805Ð811.

[24] K.W. Lawson, D.R. Lloyd, Membrane distillation, J. Membr. Sci. 124 (1997) 1Ð25.

[25] J.I. Mengual, L. Peœna, Membrane distillation, Colloid Interf. Sci. 1 (1997) 17Ð29.

[26] R.W. Schofield, A.G. Fane, C.J.D. Fell, Heat and mass transfer in membrane distillation, J. Membr. Sci. 33 (1987) 299Ð313.

[27] M. Khayet, M.P. Godino, J.I. Mengual, Theory and experiments on sweeping gas membrane distillation, J. Membr. Sci. 165 (2000) 261Ð272.

[28] F.A. Banat, J. Simandl, Theoretical and experimental study in membrane distillation, Desalination 95 (1994) 39Ð52.

[29] S. Bandini, C. Gostoli, G.C. Sarti, Separation efficiency in vacuum membrane distillation, J. Membr. Sci. 73 (1992) 217Ð229.

[30] S. Kimura, S.I. Nakao, S.I. Shimatani,Transport phenomena in membrane distillation, J. Membr. Sci. 33 (3) (1987) 285Ð298.

[31] A.M. Klaibi and N. Lior, Transport analysis in membrane distillation, Proc. IDA World Congress on Desalination and Water Reuse, Manama, Bahrain, IDA. Topsfield, MA, USA, 2002.

[32] M. Mulder, Basic Principles of Membrane Technology, 2nd ed., Kluwer, Dordrecht, 1996.

[33] ÒAn Integrated Framework for Treatment and Management of Produced Water.Ó Technical Assessment of Produced Water Treatment Technologies: RPSEA Project 07122-12. 1st edition. Colorado School of Mines. November 2009.

[34] J. Phattaranawik, R. Jiraratananon, A.G. Fane, Heat transport and membrane distillation coefficients in direct contact membrane distillation, J. Membr. Sci. 212 (2003) 177Ð193.

[35] F. Lagana, G. Barbieri, E. Drioli, Direct contact membrane distillation: modelling and concentration experiments, J. Membr. Sci. 166 (1) (2000) 1Ð11.

[36] L. Martinez-Diez, F.J. Florido-Diaz, M.I. Vazquez-Gonzalez, Study of evaporation efficiency in membrane distillation, Desalination 126 (1Ð3) (1999) 193Ð198.

[37] H. Chang, et al., Modeling and optimization of a solar driven membrane distillation desalination system, Renewable Energy 35 (12) (2010) 2714Ð2722.

[38] H. Chang, et al., Simulation of membrane distillation modules for desalination by developing user's model on Aspen Plus platform, Desalination 249 (1) (2009) 380Ð387.

[39] V.A. Bui, L.T.T. Vu, M.H. Nguyen, Modelling the simultaneous heat and mass transfer of direct contact membrane distillation in hollow fibre modules, J. Membr. Sci. 353 (1Ð2) (2010) 85Ð93.

[40] Zuo G., Energy efficiency evaluation and economic analyses of direct contact membrane distillation system using Aspen Plus, Desalination 283 (2011) 237-244.

[41] Bui V.A., et al., Simulation and optimization of direct contact membrane distillation for energy efficieny, Desalination 259 (2010) 29-39.

[42] L. Song, et al., Direct contact membrane distillation-based desalination: Novel membranes, devices, larger-scale studies, and a model, Industrial and Engineering Chemistry Research 46 (8) (2007) 2307Ð2323.

[43] Saffarini R., et al., Economic evaluation of stand-alone solar powered membrane distillation systems, Desalination 299 (2012) 55-62.

[45] S. Al-Obaidani, et al., Potential of membrane distillation in seawater desalination: Thermal efficiency, sensitivity study and cost estimation, Journal of Membrane Science 323 (1) (2008) 85-98.

8 Appendix

```
% MD Simulation: membrane module modeling

% Known values
Tfplot=zeros(1,41);
jplot =zeros(1,41);

deltaTplot=zeros(1,41);
Tpoplot=zeros(1,41);
Tfoplot=zeros(1,41);

for j = 50:90;
Tfi = j+273;                    % K, cheng
Tpi = 25+273;                   % K, cheng
L = .5;                         % m, length of membrane: approximated
x = .01;                        % m, delta(x) along length
n = L/x;                        % number of points along membrane length
Tpo = 273;                      % K, guess impossible 0 K and increase guesses
vfi = .04;                      % m/s, Zuo
vpi = .48;                      % m/s, Zuo
Amem = L*ri*2*pi;               % 0.5 m2 (Zuo is 0.3 m2)
mfi = vfi*1020*Amem;            % kg/s, density of brine = 1020 kg/m3
mpo = vpi*1000*Amem;            % kg/s, density of pure water = 1000 kg/m3
ro = 0.00063/2*1000;
ri = 0.00033/2*1000;

% Q, Tf, and Tp vectors
Q = zeros(1,n);
J = zeros(1,n);
Tf = zeros(1,n);
Tp = zeros(1,n);
mf = zeros(1,n);
mp = zeros(1,n);
Tf(1) = Tfi;
Tp(1) = Tpo;                     % guess low, now increase increments
mf(1) = mfi;
mp(1) = mpo;
Cp = 4178;                       % J/kg.K, Qtaishat

i=0;
while Tp(i+1) < Tpi;
    for i = 1:n;
        [Q(i),J(i)] = getQ(Tf(i),Tp(i));
        mf(i+1)   = mf(i)-J(i)*x*ro*2*pi;
        mp(i+1)   = mp(i)+J(i)*x*ri*2*pi;
        Tf(i+1) = getTf(Q(i),mf(i))*x+Tf(i);
        Tp(i+1) = -getTp(Q(i),mp(i))*x+Tp(i);
```

```
    end
    Tpo = Tpo + 1;
    Tp(1) = Tpo;
    Tfo = Tf(n);
    flux =((mf(1)-mf(n))/Amem)*3600;            % kg/m2h
    fprintf('Mass flow = %.5f \n',(mf(1)-mf(n)))% total transmembrane mass flow
    fprintf('Tpo = %.1f \n',Tpo)
    fprintf('Tfo = %.1f',Tfo)
end
Tfplot(j) = j;                  % Tfi
Tfoplot(j) = Tfo;               % Tfo
deltaTplot(j) = j-Tpi;          % deltaT
Tpoplot(j) = Tpo;               % Tpo
jplot(j) = flux;                % J, kg/m2h
end
plot(Tfplot,jplot,'.-')
xlabel('Feed Temperature (C)')
ylabel('Mass flux (kg/m2h)')
axis([50 90 0 60])
```

```
% Function fsolve for getQ
% Solve for Tfm, Tpm, J, Pfm, and Ppm

function F = myfun(x,Tf,Tp)
% Membrane properties
%Tf = 70+273;                    % K, cheng
%Tp = 25+273;                    % K, cheng
C = (8.6e-7)*3.6;                % kg/m2*s*Pa, MD coefficient constant for f, p.
deltaH = 2260000;                % J/kg, latent heat of vaporization

% heat transfer coefficients approximated by Qtaishat, 2008
hf = 2.623e4;                    % W/m2K
hp = 1.733e4;                    % W/m2K
hm = 784.9;                      % W/m2K, conductive heat transfer of membrane

% starting guess: Tfm, Tpm, J, Pfm, Ppm
% x(3) = 30 kg/m2h based on zuo fig.4, x(4) and x(5) = 1 bar
% x0 = [338,303,30,100000,100000];

F = [hf*(Tf-x(1))-hm*(x(1)-x(2))-deltaH*x(3);
    hp*(x(2)-Tp)-hm*(x(1)-x(2))-deltaH*x(3);
    x(3)-C*(x(4)-x(5));
    x(4)-exp(23.20-3816.44/(x(1)-46.13));
    x(5)-exp(23.20-3816.44/(x(2)-46.13))];
end
```

```
% Function getQ
% Take inputs Tfm or Tpm

function [Q,J] = getQ(Tf,Tp)
    % Values for solving Q
    hf = 2.623e4;                   % W/m2K
    %Tf = 70+273;                   % K, cheng
    hp = 1.733e4;                   % W/m2K
    hm = 784.9;                     % W/m2K, conductive membrane heat transfer
    C = (8.6e-7)*3.6;               % kg/m2*s*Pa, MD coefficient for f, p
    deltaH = 2260000;               % J/kg, latent heat of vaporization

    % call myfun.m for Tfm, Tpm
    x0 = [338,303,30,100000,100000];

    % starting guess: Tfm, Tpm, J, Pfm, Ppm
    % options = optimoptions('fsolve','iter');  % option to display output
    x = fsolve(@(x)[hf*(Tf-x(1))-hm*(x(1)-x(2))-deltaH*x(3);
    hp*(x(2)-Tp)-hm*(x(1)-x(2))-deltaH*x(3);x(3)-C*(x(4)-x(5));
    x(4)-exp(23.20-3816.44/(x(1)-46.13));
    x(5)-exp(23.20-3816.44/(x(2)-46.13))], x0);

    % call solver
    Q = hf*(Tf-x(1));
    J = x(3);

end
```

```
% Function getTf
% Take input Q to solve for Tf

function [Tf] = getTf(Q,mf)
ro = 0.00033/2*1000;      % m, outer radius, feed side
Cp = 4178;                % J/kg.K, Qtaishat
Tf = (Q*2*pi*ro)/(mf*Cp);
end
```

```
% Function getTf
% Take input Q to solve for Tp

function [Tp] = getTp(Q)
ri = 0.00033/2*1000;      % m, inner radius (zuo, chang)- permeate tube side
mf = 2.7778;              % kg/s, or 10,000 kg/hr
Cp = 4178;                % J/kg.K, Qtaishat
Tp = (Q*2*pi*ri)/(mf*Cp);
end
```